Initial electron-transfer in the reaction center from *Rhodobacter sphaeroides*

(photosynthesis/primary photoreaction/bacteriochlorophyll)

W. HOLZAPFEL[†], U. FINKELE[†], W. KAISER[†], D. OESTERHELT[‡], H. SCHEER[§], H. U. STILZ[‡], AND W. ZINTH[†]

[†]Physik Department der Technischen Universität München, 8000 Munich; [‡]Max-Planck-Institut für Biochemie, 8033 Martinsried; and [§]Botanisches Institut der Ludwig-Maximilians-Universität, 8000 Munich, Federal Republic of Germany

Contributed by Wolfgang Kaiser, April 11, 1990

ABSTRACT The initial electron transfer steps in the photosynthetic reaction center of the purple bacterium *Rhodobacter sphaeroides* have been investigated by femtosecond time-resolved spectroscopy. The experimental data taken at various wavelengths demonstrate the existence of at least four intermediate states within the first nanosecond. The difference spectra of the intermediates and transient photodichroism data are fully consistent with a sequential four-step model of the primary electron transfer: Light absorption by the special pair P leads to the state P*. From the excited primary donor P*, the electron is transferred within 3.5 ± 0.4 ps to the accessory bacteriochlorophyll B. State P^+B^- decays with a time constant of 0.9 ± 0.3 ps passing the electron to the bacteriopheophytin H. Finally, the electron is transferred from H^- to the quinone Q_A within 220 ± 40 ps.

The reaction centers (RCs) of photosynthetic bacteria are membrane-bound pigment–protein complexes (for review, see ref. 1). They mediate the conversion of light to photochemical energy through a sequence of directional electron-transfer steps across a membrane (2). Crystal structure analysis of the RCs of *Rhodopseudomonas (Rps.) viridis* (3–5) and *Rhodobacter (Rb.) sphaeroides* (6, 7) has revealed the spatial arrangement of the prosthetic groups and their protein environment. The prosthetic groups are disposed as two branches (A and B) in an approximate C2 symmetry. Two bacteriochlorophyll molecules form the so-called "special pair" (P) centered around the pseudosymmetry axis. Starting at P, each branch continues with an accessory bacteriochlorophyll (B_A or B_B), a bacteriopheophytin (H_A or H_B), and a quinone (Q_A or Q_B). A nonheme iron atom resides approximately between the two quinones close to the symmetry axis.

According to present knowledge, an electron is transferred upon light absorption from the P along branch A to the quinone Q_A (8–13). The spatial arrangement of the chromophores suggests a stepwise electron transfer via the accessory bacteriochlorophyll B_A and the bacteriopheophytin H_A (hereafter termed B and H). In this way, the sequence of radical pairs, P^+B^-, P^+H^-, and $P^+Q_A^-$, would be created.¶ Surprisingly, publications based on femtosecond spectroscopy contradicted this straightforward interpretation. It was stated (14, 15) that the electron is directly transferred from the excited special pair (P*) to H and from there to the quinone Q_A. There was no generally accepted experimental evidence of an intermediate electron-carrying state B^- (16–23). The postulated direct electron transfer from P to H imposed numerous difficulties on the theoretical description of the charge-transfer process (24–38). Various sequential reaction schemes (24–29), a nonadiabatic–adiabatic mechanism (30), or a superexchange mechanism (31–36) were considered to explain the very fast primary charge separation.

Femtosecond experiments with RCs of *Rb. sphaeroides* under optimized conditions (39) have resolved an additional kinetic component and have challenged the assumption of a 0.9-ps direct electron transfer from P to H. The appearance of a transient component suggested the existence of an intermediate state P^+B^- (39–41). Here we present data with a detailed analysis of the kinetic and spectroscopic properties of this intermediate.

Materials and Experimental Techniques

RCs from two strains of *Rb. sphaeroides*, the wild-type strain (ATCC 17023) and the carotenoid-free strain (R 26.1), were isolated as described (39). The measurements were performed at room temperature (297 K) in cuvettes with a 1-mm path length with stirring. The concentration of the samples was adjusted to OD_{860} values between 0.5 and 1.0 mm^{-1}.

A synchronously pumped unidirectional ring dye laser (42) generated pulses with a duration of 60 fs at a wavelength of 860 nm. The energy of single pulses was increased to 20 μJ by a three-stage dye amplifier (repetition rate, 10 Hz). Each of these pulses was split into two parts. (*i*) The excitation pulse was focused to a 0.5-mm spot providing an energy density of not more than 100 $\mu J/cm^2$ in the sample. In the probed volume, $\approx 7\%$ of the RCs were excited per pulse. This low excitation density prevents double excitation of the RC and related nonlinear processes. The exciting pulse, centered at 860 nm, had a bandwidth of <15 nm (full width at half-maximum). No spectral components of the exciting pulse were detected at wavelengths of <840 nm. Thus only the lowest electronic level of P at 860 nm was excited. (*ii*) The probing pulse passed an adjustable delay line and was focused onto a 1-mm-thick jet of ethylene glycol to generate a femtosecond white-light pulse. A 10- to 20-nm-wide portion of this continuum was selected by means of a special dispersion compensating monochromator (43). The energy of the probing pulses was <7 $\mu J/cm^2$.

The exciting and probing pulses were polarized either parallel or perpendicular to each other, depending on the specific experiment. If not stated otherwise, parallel polarization was used. For each probing wavelength (λ_{pr}), the instrumental response function was recorded and used in the mathematical modeling. Depending on the λ_{pr}, the temporal width (full width at half-maximum) of the instrumental response function varied between 100 fs and 200 fs, providing a temporal resolution somewhat <100 fs.

The small transmission changes resulting from the weak excitation were accurately measured by a sensitive differ-

Abbreviations: RC, reaction center; P, special pair; B, bacteriochlorophyll B_A; H, bacteriopheophytin H_A; λ_{pr}, probing wavelength.
¶Cation and anion radicals are indicated by their charges only (e.g., P^+ or H^-).

ence-detection system (44). At least 1000 individual absorption data were taken for each delay time t_D.

A series of control experiments was carried out as follows: (i) RCs from two strains (ATCC 17023 and R 26.1) were investigated. Experiments performed at 665 and 920 nm gave identical results for both samples. (ii) Additional experimental runs were made at a λ_{pr} of 665 nm with reduced excitation intensity to exclude irradiance artifacts. The same kinetic constants were observed when <2% of the RCs were excited instead of 7%. (iii) It was ascertained in two ways that no long-lived intermediates accumulated during the experiments: (a) The transmission of the sample was continuously recorded at the excitation wavelength of 860 nm and no long-term absorption changes occurred. (b) The time-resolved data shown in Figs. 1 and 3 were obtained from at least 10 individually recorded traces. The latter were found not to be influenced by the integral exposure of the sample. (iv) To rule out sample decomposition, the absorption spectra were recorded prior to and after each experiment. No indicative absorption changes were found.

Theoretical Analysis of the Data

The mathematical description of the transient absorption changes is based on the hypothesis that intermediates with spectroscopically well-defined properties exist. The excitation of the RC in its ground state I_0 leads to the population of a first intermediate state I_1. Subsequent decay processes populate intermediates I_2–I_n. The population changes of the intermediate states are determined by the rate equation system:

$$\frac{dN_i(t)}{dt} = -\sum_{j=1}^{n} K_{ij}N_j(t) \quad \text{for } i = 1 \ldots n, \quad [1]$$

where the rate constants K_{ij} for $i \neq j$ describe the population transfer from intermediate I_j to I_i. For the most probable case of nondegenerate eigenvalues of the rate constant matrix, K_{ij}, the population density $N_i(t)$ of a state I_i, is a linear combination of n exponentials:

$$N_i(t) = \sum_{j=1}^{n} N_{ij}e^{-k_jt} \quad \text{for } t > 0$$

and   [2]

$$N_0(t) = N - \sum_{i=1}^{n} N_i(t).$$

The decay constants k_j are the eigenvalues of the rate constant matrix K_{ij}. The matrix N_{ij} may be calculated from the eigenvectors of the rate constant matrix K_{ij} and the starting population $N_i(0)$. N is the total density of RCs.

For weak excitation, the duration of the exciting and probing light pulses is taken into account by the instrumental response function $R(t)$, which is the measured cross correlation of probing and exciting intensities. In this way, the exponentials in Eq. 2 are replaced by the functions $F_j(t)$.

$$F_j(t) = \int_0^\infty dt'R(t - t')e^{-k_jt'}. \quad [3]$$

Finally, the absorbance change of a sample of thickness ℓ detected at a delay time (t_D) becomes

$$\Delta A(\lambda_{pr},t_D) = \frac{1}{\ln 10}\sum_{j=1}^{n}\sum_{i=1}^{n}[\sigma_i(\lambda_{pr}) - \sigma_0(\lambda_{pr})]N_{ij}F_j(t_D)\ell$$

$$= \sum_{j=1}^{n} a_j(\lambda_{pr})F_j(t_D). \quad [4]$$

Eq. 4 shows that a transient absorption measurement provides a set of amplitudes a_j and decay constants k_j contained in F_j. In a general case, where branching and back reactions occur, it is not possible to reconstruct the complete rate constant matrix K_{ij} without additional information. In the special case of a linear sequential reaction model, the information obtained from transient spectroscopy is sufficient to calculate the rate constant matrix K_{ij} and the difference spectra $[\sigma_i(\lambda_{pr}) - \sigma_0(\lambda_{pr})]$ of the intermediates without free parameters.

As a consequence of Eq. 4, the most rapid decay process always appears close to time zero, even if the related intermediate occurs at a later stage in the reaction scheme. The amplitudes $a_j(\lambda_{pr})$ of the exponentials, however, strongly depend on the rate constants and on the order of states.

It should be noted that the determination of the decay rates τ_i and amplitudes $a_i(\lambda_{pr})$ from the transient experimental data are independent of the specific model, whereas the calculation of the difference spectra depends on the assumed reaction model.

Results

The time-resolved absorption changes were measured at λ_{pr} values between 500 and 1000 nm. Data at a λ_{pr} of >860 nm give information on the ground-state species P and the excited electronic state P* (18). The accessory B has its Q_y and Q_x transitions at λ_{pr} values of 805 and 600 nm, respectively. The Q_y and Q_x transitions of H occur at 760 nm and 540 nm, respectively. Of special interest is the spectral region around 670 nm, where the unexcited RCs absorb only weakly but where the reduced B⁻ molecules (45) and the reduced H⁻ molecules (46) have a pronounced absorption.

In Fig. 1 the transient absorption changes are plotted for λ_{pr} values of 920 nm, 785 nm, and 545 nm. At early delay times ($t_D < 1$ ps), a linear time scale and, for later times ($t_D > 1$ ps), a logarithmic scale is used. The broken curves are calculated according to a kinetic model including three decay times $\tau_j = 1/k_j$ of 3.5 ps, 220 ps, and ∞. ∞ corresponds to a constant absorption on the investigated time scale of 1 ns. A fourth kinetic component with a decay time of 0.9 ps is added to compute the solid curves in Fig. 1 *b* and *c*.

At a λ_{pr} of 920 nm (Fig. 1a), one sees a nearly instantaneous decrease of absorption due to the formation of the excited state P*. Induced emission (gain) from P* and depopulation of the ground state P contribute to the absorption decrease. The subsequent relaxation of the signal with a time constant of 3.5 ± 0.4 ps represents the decay of P*. At t_D values of >10 ps, the absorption again slightly decreases due to the formation of the long-lived final photoproduct $P^+Q_A^-$, which absorbs less than the initial ground state. The three-component model (broken curve) readily describes the observed absorption changes at this λ_{pr} of 920 nm.

At a λ_{pr} of 785 nm, enhanced absorption is observed throughout the entire time range (Fig. 1b). The absorption rapidly increases around time zero to a maximum followed by a decrease with a time constant of 0.9 ± 0.3 ps between 0.2 and 2 ps. At later delay times, the absorption increases again with two different time constants of ≈3.5 ps and 220 ps. In contrast to the measurements at a λ_{pr} of 920 nm (Fig. 1a), the three-component model (broken curve) cannot describe the observed absorption changes at a λ_{pr} of 785 nm. A fourth kinetic component with a decay time of 0.9 ps is required for a satisfactory fit of the data (solid curve in Fig. 1b). The necessity of the fourth kinetic component is also clearly seen at other λ_{pr} values of 545 nm (Fig. 1c), 665 nm (see Fig. 3, solid circles), and 775 nm (data not shown).

At a λ_{pr} of 545 nm, the absorption rises as a result of the formation of P* to a broad maximum (Fig. 1c). The plateau between t_D values of 0.1 ps and 1 ps originates from the 0.9-ps kinetic component. Omission of this component would lead
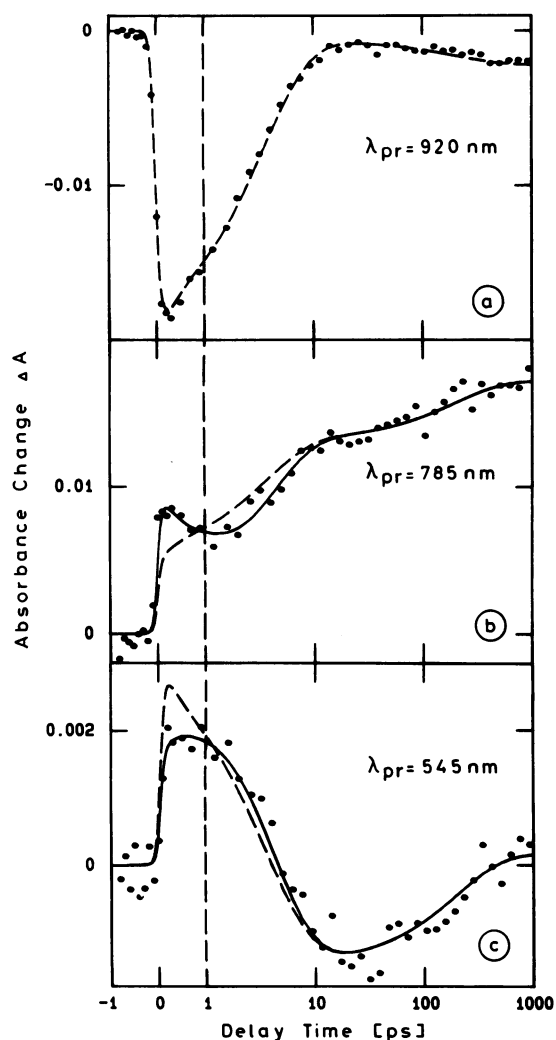
FIG. 1. Time-resolved absorption data (solid circles) for λ_{pr} values of 920 nm (*a*), 785 nm (*b*), and 545 nm (*c*) for RCs of *Rb. sphaeroides* strains, ATCC 17023 (*a* and *b*) and R 26.1 (*c*) [excitation wavelength, 860 nm]. The curves are calculated according to the models discussed in the text. Broken curves, calculated according to a kinetic model with three decay times; solid curves, calculated according to a kinetic model with four decay times.

FIG. 2. Amplitude spectra $a_j(\lambda_{pr})$ of the four kinetic components τ_1-τ_4. The data points represent the amplitudes $a_j(\lambda_{pr})$ of the four components with time constants of 3.5 ps (a_1), 0.9 ps (a_2), 220 ps (a_3), and ∞ (a_4) used to fit the transient absorption data at the various values of λ_{pr}. The solid lines were drawn to guide the eye. At λ_{pr} values <720 nm, all amplitudes are multiplied by a factor of 4. At λ_{pr} values >600 nm, RCs from strain ATCC 17023 and at λ_{pr} values <600 nm RCs from strain R26.1 were used.

to an immediate decay of the absorption, as indicated by the broken line. The strong absorption decrease between 1 and 10 ps results from the reduction of H. At late t_D values, the absorption rises again, when the electron is transferred from H^- to Q_A.

Time-dependent measurements were carried out at more than 20 values of λ_{pr}. The analysis of this large body of data concludes that the smallest number n of intermediate states is $n = 4$.‖ The related time constants, consistent with all data curves, are $\tau_1 = 3.5 \pm 0.4$ ps, $\tau_2 = 0.9 \pm 0.3$ ps, $\tau_3 = 220 \pm 40$ ps, and $\tau_4 = \infty$. In Fig. 2, the amplitude spectra $a_j(\lambda_{pr})$ are presented. They are used below to relate the different kinetic components to specific intermediate states of the RCs.

At λ_{pr} values of 665 nm (Fig. 3) and 753 nm (data not shown), the transient absorption changes were investigated for parallel and perpendicular polarizations of probing and exciting pulses. A pronounced dichroism is induced by the exciting light pulses at both wavelengths.

‖Within the experimental accuracy, a weak fifth component with a time constant of between 10 and 20 ps cannot be ruled out. This component, if it exists, provides further complication but does not interfere with the present conclusions.
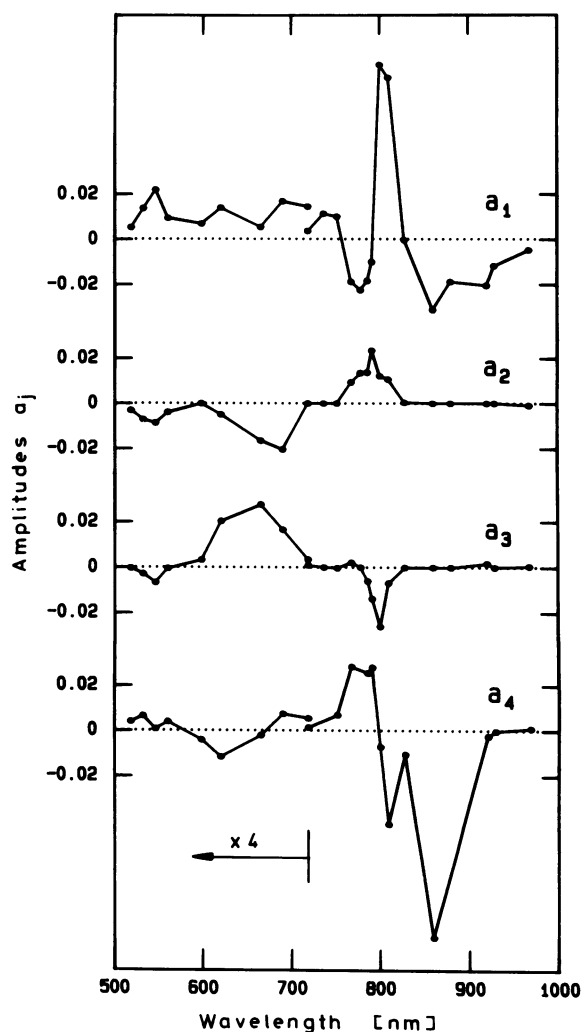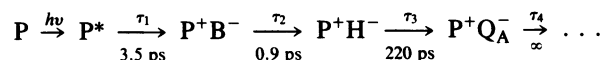
Discussion

The experimental data strongly suggest the existence of the four time constants 0.9 ps, 3.5 ps, 220 ps, and ∞ with the amplitude spectra of Fig. 2. Four intermediate states, I_1-I_4, are connected with these four time constants. Difference spectra ($\sigma_i - \sigma_0$) of the intermediates may be determined from the experimental results, if the reaction scheme is known. It is accepted that light absorption generates the electronically excited state P* and that the states related with the time constants of 220 ps and ∞ are P^+H^- and $P^+Q_A^-$, respectively (11, 18, 20, 47–49). As a consequence the difference spectra for these three states can be calculated from the data of Fig. 2. The determination of the difference spectrum of the second intermediate requires the assumption of a specific model for the primary reaction. The structure of the RC suggests a stepwise electron transfer along the chromophores:

$$P \xrightarrow{h\nu} P^* \xrightarrow[3.5 \text{ ps}]{\tau_1} P^+B^- \xrightarrow[0.9 \text{ ps}]{\tau_2} P^+H^- \xrightarrow[220 \text{ ps}]{\tau_3} P^+Q_A^- \xrightarrow[\infty]{\tau_4} \ldots$$

The order of the time constants is based on the following argument: The occupation of the electronically excited level
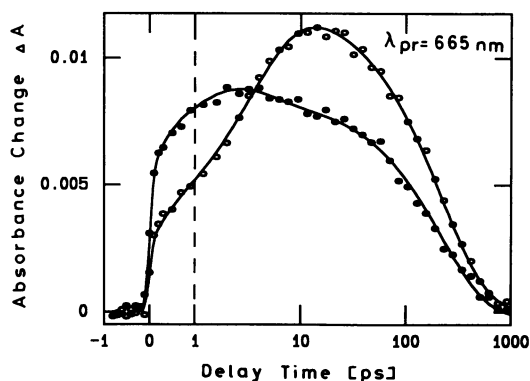
FIG. 3. Polarized time-resolved absorption data taken at a λ_{pr} of 665 nm for RCs of *Rb. sphaeroides* ATCC 17023. The polarizations of exciting and probing pulses are parallel (solid circles) or perpendicular (open circles). The calculated curves (solid lines) are based on the four-component model discussed in the text.

P* is reflected by optical gain, which decays with a time constant of 3.5 ps. Consequently, the 3.5-ps component may be linked to the first step in the sequence, and the shorter, the 0.9-ps kinetic, is the second step. By using this order of intermediates, the difference cross-section spectra of the states I_1–I_4 were calculated (Fig. 4a). These spectra are difference spectra of the intermediates I_j and the ground state. They should not be mixed up with common experimental transient spectra, which reflect the mixture of the various intermediates being populated at any chosen t_D value. The data shown in Fig. 4a are calculated from the experimental data. For wavelengths of <720 nm, the values are enlarged for better display. The calculation of the difference spectra ($\sigma_i - \sigma_0$) is based on measurements, where the exciting and probing pulses were polarized parallel.

The difference spectrum of the final photoproduct I_4 [$P^+Q_A^-$, ($\sigma_4 - \sigma_0$), Fig. 4a] reflects the disappearance of the P-absorption (negative values around 860 nm and 600 nm) and the electrochromic shift due to the radical pair P^+Q^- (dispersive shape in the Q_y band of the monomeric bacteriochlorophyll around 800 nm). The difference spectrum of the photoproduct I_3 [P^+H^-, ($\sigma_3 - \sigma_0$), Fig. 4a], with a decay time of 220 ps, resembles the one of $P^+Q_A^-$. Differences between the spectra originate from the reduction of H. Especially the pronounced absorption increase around 660 nm is due to the absorption of H^-. On the other hand, in the Q_y band of H (760 nm), no absorption decrease is found for parallel polarized pulses due to the particular orientation of the Q_y transition moment. The difference spectrum of the first intermediate I_1 [P*, ($\sigma_1 - \sigma_0$), Fig. 4a] strongly deviates from the other difference spectra. Due to stimulated emission (gain) of P*, the absorption decrease at λ_{pr} values >830 nm is larger and extends further to the infrared. Between 750 and 830 nm, a strong absorption increase peaking at 800 nm is observed, which is caused by strong absorption of the excited state P*.

Of special interest is the difference spectrum of the intermediate I_2 with a decay time of 0.9 ps. It shows the same absorption decrease in the P band at 860 nm as the intermediates I_3 and I_4, emphasizing that intermediate I_2 also contains an oxidized P^+. The absorption decrease at 805 nm is stronger than that of I_3 and I_4 by >50%. The band is broadened toward shorter wavelengths. In contrast to the spectra of intermediates I_3 and I_4, there is no dispersive shape in the range of the Q_y band of the accessory B around 800 nm. Instead, the spectrum indicates a partial bleach of the monomeric B band. Between 700 and 500 nm, where B^- and H^- absorb strongly, a rather intense absorption increase occurs, which around 665 nm is nearly three times larger than in the intermediate I_3 (P^+H^-). The minimum around 600 nm reflects
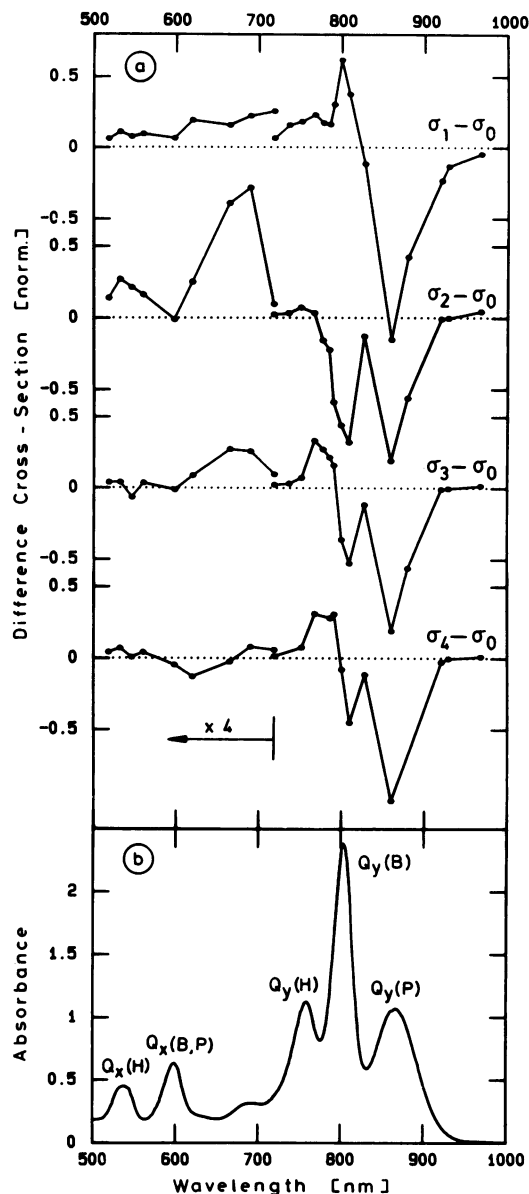

FIG. 4. (a) Spectra of the difference cross-sections ($\sigma_i - \sigma_0$) of the four intermediates P* (σ_1), P^+B^- (σ_2), P^+H^- (σ_3), and $P^+Q_A^-$ (σ_4) relative to the cross-section of the ground state (σ_0). The data (solid circles) are calculated from the amplitude spectra of Fig. 2, assuming the four-component sequential model. (b) Absorbance spectrum of the ground-state RCs of *Rb. sphaeroides* R26.1 proportional to σ_0.

the disappearance of a bacteriochlorophyll Q_x absorption. These spectral features support the hypothesis that intermediate I_2 contains a reduced monomeric B molecule.

The above interpretation is strongly supported by the time-resolved dichroism data at 665 nm (Fig. 3). From these experimental data the values of $\Delta\sigma_\perp/\Delta\sigma_\parallel$ of the intermediates I_2 and I_3 were calculated to be 0.59 ± 0.2 and 1.46 ± 0.06, respectively. Based on these values the angles Θ between the transition moments of the P band at 860 nm and the transition moment of the species absorbing at 665 nm were evaluated (50). For intermediate I_2, a value of $\Theta_2 = 36°$ (19°–46°) and, for I_3, a value of $\Theta_3 = 68 ± 2°$ were obtained. These numbers should be compared with the corresponding angles calculated from the protein structure.** Quantum-chemical calculations

---

**The directions of the Q_y transition of the tetrapyrol was assumed to be parallel to the line connecting the nitrogens of ring 1 and ring 3.

have shown that the 660-nm bands of bacteriochlorophyll a and of bacteriopheophytin a anion radicals (51, 52) are practically parallel to the Q_y transition of the unreduced molecules. The high-resolution (2.3 Å) structure of the RCs of *Rps. viridis* was employed as a model for *Rb. sphaeroides* to calculate values of $\Theta_B = 29°$ for the accessory B and $\Theta_H = 73°$ for the H. This finding is in good agreement with our experimental values and confirms that the 665-nm absorption band of intermediate I_2 is due to a reduced B molecule and not due to a reduced H molecule.

The analysis of the transient absorption changes given above was based on the model where one excited state P* decays through a linear sequence of radical pairs. It describes the experimental data and is fully supported by model calculations (53). Even though, other schemes cannot be excluded. Two possible alternatives are as follows. (*i*) A branched reaction model, where the formation of P^+H^- occurs either through the radical pair state P^+B^- or directly through a superexchange mechanism (fraction η). However, the photodichroism data restrict the value of η to <0.5. (*ii*) A model with two excited states, P_1^* and P_2^*, with relaxation times of 0.9 and 3.5 ps, respectively. At present there is no support for the existence of two excited electronic states of P.

In conclusion, femtosecond spectroscopy on the RCs of *Rb. sphaeroides* demonstrates that at least four time constants are related to the primary electron transfer during the first nanosecond. The experimental data—time-dependent absorption changes, difference spectra of the intermediates, and photodichroism—are in full agreement with the model of a stepwise electron transfer suggested by the chromophore arrangement: After excitation of the P, an electron is transferred to the accessory B within 3.5 ps. Here the electron resides for 0.9 ps before it is transferred to the H. With a time constant of 220 ± 40 ps, it finally arrives at the quinone Q_A.

1. Parson, W. W. (1982) *Annu. Rev. Biophys. Bioeng.* **11**, 57–80.
2. Hochstrasser, R. M. & Johnson, C. K. (1988) in *Ultrashort Laser Pulses*, ed. Kaiser, W. (Springer, Berlin), pp. 357–417.
3. Deisenhofer, J., Epp, O., Miki, K., Huber, R. & Michel, H. (1984) *J. Mol. Biol.* **180**, 385–398.
4. Michel, H., Epp, O. & Deisenhofer, J. (1986) *EMBO J.* **5**, 2445–2451.
5. Deisenhofer, J. & Michel, H. (1989) *EMBO J.* **8**, 2149–2170.
6. Chang, C.-H., Tiede, D., Tang, J., Smith, U., Norris, J. & Schiffer, M. (1986) *FEBS Lett.* **205**, 82–86.
7. Allen, J. P., Feher, G., Yeates, T. O., Komiya, H. & Rees, D. C. (1987) *Proc. Natl. Acad. Sci. USA* **84**, 5730–5734.
8. Zinth, W., Knapp, E. W., Fischer, S. F., Kaiser, W., Deisenhofer, J. & Michel, H. (1985) *Chem. Phys. Lett.* **119**, 1–4.
9. Kirmaier, C., Holten, D. & Parson, W. W. (1985) *Biochim. Biophys. Acta* **810**, 33–48.
10. Kaufmann, K. J., Dutton, P. L., Netzel, T. L., Leigh, J. S. & Rentzepis, P. M. (1975) *Science* **188**, 1301–1304.
11. Rockley, M. G., Windsor, M. W., Cogdell, R. J. & Parson, W. W. (1975) *Proc. Natl. Acad. Sci. USA* **72**, 2251–2255.
12. Holten, D., Windsor, M. W., Parson, W. W. & Thornber, J. P. (1978) *Biochim. Biophys. Acta* **501**, 112–126.
13. Holten, D., Hoganson, C., Windsor, M. W., Schenck, C. C., Parson, W. W., Migus, A., Fork, R. L. & Shank, C. V. (1980) *Biochim. Biophys. Acta* **592**, 461–477.
14. Martin, J.-L., Breton, J., Hoff, A. J., Migus, A., Antonetti, A. (1986) *Proc. Natl. Acad. Sci. USA* **83**, 957–961.
15. Breton, J., Martin, J.-L., Migus, A., Antonetti, A., Orszag, A. (1986) *Proc. Natl. Acad. Sci. USA* **83**, 5121–5125.
16. Shuvalov, V. A. & Klevanik, A. V. (1983) *FEBS Lett.* **160**, 51–55.
17. Shuvalov, V. A., Amesz, J. & Duysens, L. N. M. (1986) *Biochim. Biophys. Acta* **851**, 327–330.
18. Woodbury, N. W., Becker, M., Middendorf, D. & Parson, W. W. (1985) *Biochemistry* **24**, 7516–7521.
19. Becker, M., Middendorf, D., Woodbury, N. W., Parson, W. W. & Blankenship, R. E. (1986) in *Ultrafast Phenomena V*, Springer Series in Chem. Phys., eds. Fleming, G. R. & Siegman, A. E. (Springer, Heidelberg), pp. 374–378.
20. Chekalin, S. V., Matveets, Y. A. & Yartsev, A. P. (1986) in *Ultrafast Phenomena V*, Springer Series in Chem. Phys., eds. Fleming, G. R. & Siegman, A. E. (Springer, Heidelberg), pp. 402–405.
21. Wasielewski, M. R. & Tiede, D. M. (1986) *FEBS Lett.* **204**, 368–372.
22. Breton, J., Martin, J.-L., Petrich, J., Migus, A., Antonetti, A. (1986) *FEBS Lett.* **209**, 37–43.
23. Fleming, G. R., Martin, J.-L. & Breton, J. (1988) *Nature (London)* **333**, 190–192.
24. Haberkorn, R., Michel-Beyerle, M. E. & Marcus, R. A. (1979) *Proc. Natl. Acad. Sci. USA* **76**, 4185–4188.
25. Marcus, R. A. (1987) *Chem. Phys. Lett.* **133**, 471–477.
26. Marcus, R. A. (1988) in *The Photosynthetic Bacterial Reaction Center: Structure and Dynamics*, eds. Breton, J. & Vermeglio, A. (Plenum, New York), pp. 389–398.
27. Scherer, P. O. J. & Fischer, S. F. (1987) *Chem. Phys. Lett.* **141**, 179–185.
28. Fischer, S. F. & Scherer, P. O. J. (1987) *Chem. Phys.* **115**, 151–158.
29. Scherer, P. O. J. & Fischer, S. F. (1989) *Chem. Phys.* **131**, 115–127.
30. Marcus, R. A. (1988) *Chem. Phys. Lett.* **146**, 13–22.
31. Bixon, M., Jortner, J., Michel-Beyerle, M. E., Ogrodnik, A. & Lersch, W. (1987) *Chem. Phys. Lett.* **140**, 626–630.
32. Bixon, M., Michel-Beyerle, M. E. & Jortner, J. (1988) *Israel J. Chem.* **28**, 155–168.
33. Ogrodnik, A., Remy-Richter, N., Michel-Beyerle, M. E. & Feick, R. (1987) *Chem. Phys. Lett.* **135**, 576–581.
34. Michel-Beyerle, M. E., Plato, M., Deisenhofer, J., Michel, H., Bixon, M. & Jortner, J. (1988) *Biochim. Biophys. Acta* **932**, 52–70.
35. Plato, M., Möbius, K., Michel-Beyerle, M. E., Bixon, M. & Jortner, J. (1988) *J. Am. Chem. Soc.* **110**, 7279–7285.
36. Michel-Beyerle, M. E., Bixon, M. & Jortner, J. (1988) *Chem. Phys. Lett.* **151**, 188–194.
37. Warshel, A., Creighton, S. & Parson, W. W. (1988) *J. Phys. Chem.* **92**, 2696–2701.
38. Creighton, S., Hwang, J.-K., Warshel, A., Parson, W. W. & Norris, J. (1988) *Biochemistry* **27**, 774–781.
39. Holzapfel, W., Finkele, U., Kaiser, W., Oesterhelt, D., Scheer, H., Stilz, H. U. & Zinth, W. (1989) *Chem. Phys. Lett.* **160**, 1–7.
40. Zinth, W., Holzapfel, W. & Finkele, U. (1989) in *Spectroscopy of Biological Molecules—State of the Art*, eds. Bertoluzza, A., Fagnano, G. & Monti, P. (Soc. Editrice Esculapio, Bologna, Italy) pp. 291–294.
41. Zinth, W., Holzapfel, W., Finkele, U., Kaiser, W., Oesterhelt, D., Scheer, H. & Stilz, H. U. (1990) *Current Research in Photosynthesis*, ed. Baltscheffsky, M. (Kluwer, Dordrecht) Vol. 1, pp. I.1.27–I.1.30.
42. Dobler, J., Schulz, H. H. & Zinth, W. (1986) *Optics Commun.* **57**, 407–409.
43. Martinez, O. E. (1987) *IEEE J. Quant. Electron.* **23**, 59–64.
44. Polland, H. J. & Zinth, W. (1985) *J. Phys. E.* **18**, 399–400.
45. Fajer, J., Borg, D. C., Forman, A., Dolphin, D. & Felton, R. H. (1973) *J. Am. Chem. Soc.* **95**, 2739–2741.
46. Fajer, J., Davis, M. S., Brune, D. C., Spaulding, L. D., Borg, D. C. & Forman, A. (1976) *Brookhaven Symp. Biol.* **28**, 74–104.
47. Schenck, C. C., Parson, W. W., Holten, D. & Windsor, M. W. (1981) *Biochim. Biophys. Acta* **635**, 383–392.
48. Kirmaier, C., Holten, D. & Parson, W. W. (1983) *Biochem. Biophys. Acta* **725**, 190–202.
49. Kirmaier, C., Holten, D. & Parson, W. W. (1985) *Biochem. Biophys. Acta* **810**, 49–61.
50. Vermeglio, A., Breton, J., Paillotin, G. & Cogdell, A. (1978) *Biochim. Biophys. Acta* **501**, 514–530.
51. Petke, J. D., Maggiora, G. M., Shipman, L. L. & Christoffersen, R. E. (1981) *Photochem. Photobiol.* **33**, 663–671.
52. Petke, J. D., Maggiora, G. M., Shipman, L. L. & Christoffersen, R. E. (1980) *Photochem. Photobiol.* **32**, 661–667.
53. Parson, W. W., Chu, Z. T. & Warshel, A. (1990) *Biochim. Biophys. Acta*, in press.